

RESEARCH

Open Access



Compound probiotics alleviate hyperuricemia-induced renal injury via restoring gut microbiota and metabolism

Ping Liu^{1†}, Ping Hu^{1†}, Meiping Jin¹, Weiqian Sun¹, Jiajun Wu¹, Yuyan Tang¹, Danye Shi¹, Ting Xie¹, Yijing Tong¹, Lusheng Huang¹, Dongliang Zhang¹, Hui Zheng^{2*}, Xudong Xu^{1*} and Haidong He^{1*}

Abstract

To investigate the role and mechanisms of gut microbiota in hyperuricemia-induced renal injury, we established renal failure models using unilateral nephrectomized mice. After four weeks of adenine and potassium oxalate-supplemented diet, probiotic intervention was administered. Renal pathological and functional changes were assessed through H&E staining and plasma biochemical analysis. Gut microbiota composition and metabolite profiles were evaluated using 16 S rRNA gene sequencing and non-targeted metabolomics of fecal samples. Our findings demonstrate that the compound probiotics effectively attenuated hyperuricemia-associated renal dysfunction and interstitial fibrosis. The intervention reduced oxidative stress, mitophagy, and apoptosis in renal tubules. Probiotic treatment enhanced gut microbiota diversity, notably increasing the abundance of *Prevotella_9*, *Dorea*, and unclassified *Bacteroidota*, while decreasing unclassified *Desulfovibrio*. KEGG enrichment analysis revealed that probiotic intervention upregulated arginine and proline metabolism, as well as tyrosine metabolism in feces. Furthermore, it enhanced the metabolism of arginine, proline, valine, leucine, and isoleucine in plasma. Notably, sulfocholic acid and urocanic acid showed negative correlations with oxidative stress markers, autophagy, and apoptosis indicators. Similarly, plasma L-proline levels were inversely correlated with these pathological parameters. These results suggest that the compound probiotics may mitigate hyperuricemia-induced kidney damage through restoration of gut microbiota homeostasis and preservation of plasma and fecal metabolites. The protective mechanisms likely involve attenuation of hyperuricemia-associated oxidative stress, mitochondrial dysregulation, and phagocytosis-induced apoptosis. Our study provides compelling evidence that probiotic supplementation represents a promising therapeutic strategy for hyperuricemia-induced renal injury, potentially through modulation of gut microbiota and associated metabolic pathways.

[†]Ping Liu and Ping Hu contributed equally to this work and are co-first authors.

*Correspondence:

Hui Zheng
zheng_hui@fudan.edu.cn
Xudong Xu
xxdmzx@sina.com
Haidong He
chinahhd@sina.com

Full list of author information is available at the end of the article



Keywords Compound probiotics, Uric acid nephropathy, Metabolomics, Amino acid metabolism

Clinical trial number

Not applicable.

Introduction

In recent years, the global prevalence of hyperuricemia (HUA) has increased significantly, the overall incidence rate of HUA in China has risen to 15.1%, posing a new public health challenge [1, 2]. Hyperuricemia is a chronic metabolic disorder resulting from the dysregulation of purine metabolism. It occurs when the production of uric acid exceeds its excretion. Typically, the kidneys excrete approximately 70% of the daily produced UA, while the remaining 30% is eliminated via the intestine [3]. Increasing evidence suggests that high uric acid levels play a direct role in the pathophysiology of chronic kidney disease (CKD) [4]. The prevalence of uric acid nephropathy has increased in recent years, posing a considerable health and economic burden and serious health and financial risk. To reduce the disease burden, it is essential to develop methods that effectively stop the progression of urinary acid nephropathy and improve renal function.

Persistent hyperuricemia damage to the kidney has been shown to induce tubular damage, interstitial fibrosis, glomerulosclerosis, and urate crystal deposition, resulting in hyperuricemic nephropathy [5, 6]. One significant mechanism through which hyperuricemia contributes to CKD is mitochondrial dysfunction. Research has demonstrated that the kidney, being a highly oxygen-consuming organ, can experience tubular epithelial dysfunction due to the oxidant urate, which increases mitochondrial superoxide production. Excessive reactive oxygen species (ROS) production can then harm mitochondrial DNA and the electron transport chain [7].

In damaged mitochondria's outer membrane, certain members of the BCL2 protein family, like Bax, can facilitate the release of cytochrome c into the cytoplasm, initiating a caspase-dependent apoptotic signaling cascade that leads to apoptosis, resulting in tubular atrophy and nephron loss [8, 9]. Prolonged hyperuricemia can also trigger sustained autophagy in proximal tubules, causing irreversible collapse of tubular epithelial cell viability and loss of cell protection, thus accelerating the progression of interstitial fibrosis [10].

The gut microbiota has been associated with various metabolic diseases, including HUA. Numerous probiotics have been found to lower serum uric acid (SUA) levels through different mechanisms. For instance,

Lactobacillus gasseri PA-3 was initially discovered to absorb and utilize purines directly in vitro [11]. Subsequently, it was observed to reduce SUA by competing for purine absorption in the rat intestine, leading to decreased purine absorption in rats [12]. Additionally, *Lactobacillus paracasei* X11 has shown beneficial effects on restoring intestinal flora [13]. *Lactobacillus brevis* DM9218 has been found to decrease SUA levels in fruit-fed mice [14]. Both *Lactobacillus reuteri* TSR332 and *Lactobacillus fermentum* TSF331 have been demonstrated to lower SUA levels in rats without any evident side effects during treatment [15]. *Lactobacillus fermentum* F40-4 can modulate xanthine oxidase levels and uric acid transporter expression, thereby ameliorating HUA [16]. *Lactococcus* D2022 can reduce SUA concentration and regulate uric acid excretion by inhibiting UA synthesis. Studies have indicated that D2022 may alleviate HUA-induced renal injury, possibly due to increased short-chain fatty acids (SCFA) in the intestine and alterations in free fatty acid receptor (FFAR) expression resulting in decreased NLRP3 inflammasome pathway expression [17]. Li et al. utilized *Faecalibacterium prausnitzii* to intervene in CKD mice, successfully altering the mice's intestinal flora structure and improving renal dysfunction, inflammation, and various uremic toxin levels in the serum [18]. These findings suggest that probiotics hold promise in managing hyperuricemia and slowing the progression of CKD. Nonetheless, there is a scarcity of research on the impact of probiotics on renal function and potential mechanisms in uric acid nephropathy.

The gut-kidney axis theory provides a comprehensive explanation for the bidirectional communication between gut microbiota and kidney disease. Changes in the gastrointestinal tract or kidneys can influence each other through various pathways, such as energy metabolism, pro-inflammatory immune response, intestinal mucosa, and intestinal flora [19, 20]. Previous studies have shown significant differences in intestinal flora and metabolite bacteria in patients with CKD combined with HUA [21]. Metabolomic studies in UOX-KO mice have confirmed alterations in purine metabolism, amino acid biosynthesis, tryptophan metabolism, and neuroactive ligand-receptor interactions. Betaine and biotin have been identified as potential plasma metabolism biomarkers for predicting urateuric acid nephropathy

and are associated with renal function [22]. Investigating the metabolite changes induced by probiotics in the context of uric acid nephropathy pathogenesis is crucial. We hypothesize that the beneficial effects of probiotics in attenuating uric acid nephropathy progression may be linked to specific changes in metabolites within the body. Identifying these changes could offer valuable insights into the mechanisms through which probiotics improve uric acid nephropathy.

This study aims to investigate the beneficial effects of different probiotic combinations on the prevention and management of uric acid nephropathy by modulating oxidative stress and mitophagy in the kidneys. Utilizing both normal and hyperuricemia mouse models, the study assessed the impact of probiotics in ameliorating local inflammation and fibrosis in the kidneys. Furthermore, through the analysis of gut microbiota and metabolomics, the study elucidated the influence of probiotics on the structure and metabolism of intestinal flora in the mice. Additionally, correlation analysis was employed to preliminarily establish the link between gut microbiota, metabolites, kidney function, and mitophagy. These findings offer a promising therapeutic approach for addressing uric acid nephropathy within the context of chronic kidney disease.

Materials and methods

Animal model and treatment conditions

SPF-grade male C57BL/6 mice, aged 8 weeks, were procured from Shanghai Slack Laboratory Animal Company and maintained in a controlled environment (average temperature of 22 °C, standard 12-hour light/dark cycle, and relative humidity of 40–60%). The mice were provided with free access to water and food. In this experiment, a hyperuricemic mouse model was constructed using exogenous uric acid precursors (adenine) and uricase activity inhibitors (potassium oxonate), combined with unilateral nephrectomy to establish a model of uric acid nephropathy.

Following a one-week adaptive feeding, unilateral nephrectomy was performed to establish a chronic kidney disease (CKD) animal model ($n=12$). A sham operation was conducted concurrently ($n=6$) without nephrectomy. Post-surgery, the mice were observed for an additional two weeks. They were categorized into three experimental groups: (1) sham operation group ($n=6$), which received the same volume of CMC-Na as the control group orally, once daily; (2) UNx+HPD group, which received daily suspensions of adenine (0.1 g/kg) and potassium oxonate (1.5 g/kg); and (3) UNx+HPD+P group, which received daily suspensions of adenine (0.1 g/kg) and potassium oxonate (1.5 g/kg), along with mixed probiotics (5×10^9 CFU) administered daily. All mice underwent the aforementioned treatments

for nine weeks before being euthanized using CO₂. The flowchart of the treatment for mice is shown in Fig. 1A.

The mixed probiotic freeze-dried powder agent contains 2.2×10^{10} CFU of live bacteria per bag, donated by Zhongke Yikang Biotechnology Co., Ltd. Product formula: 6 kinds of *Bifidobacteria*: *Bifidobacterium lactis* HN019, *Bifidobacterium bifidum* Bb-06, *Bifidobacterium animalis* BB-12, *Bifidobacterium lactis* Bi-i07, *Bifidobacterium longum* R175, *Bifidobacterium animalis* B94. 8 species of *Lactobacilli*: *Lactobacillus rhamnosus* GG, *Lactobacillus casei* LC11, *Lactobacillus helveticus* R52, *Lactobacillus paracasei* Lpc37, *Lactobacillus plantarum* R1012, *Lactobacillus reuteri* HA188, *Lactobacillus rhamnosus* R11, and *Lactobacillus acidophilus* NCFM. 1 type of *Streptococcus*: *Streptococcus thermophilus* St21.3 types of prebiotics: inulin, galacto-oligosaccharide, and fructooligosaccharide.

Sample collection

Blood was drawn from the medial canthal vein at the end of the experiment. Serum samples were separated by centrifugation at 1200 g for 10 min at 4 °C and subsequently stored at -80 °C. Intact kidneys were removed, washed with phosphate-buffered saline (PBS; pH=7.2–7.3), fixed in fresh 4% paraformaldehyde, and embedded in paraffin. Colon feces were collected and refrigerated at -80 °C.

Biochemical analysis

Serum creatinine (SCR), blood urea nitrogen (BUN) and blood uric acid were measured by biochemical kits (Nanjing Chengjian Bioengineering Research Institute; C012-2-1). Malondialdehyde (MDA) and superoxide dismutase (SOD) analyzed by Commercial kits (Nanjing Chengjian Bioengineering Research Institute; A003-1-2/A001-3-2).

Histopathological assessments of the kidneys

The kidneys were fixed in 10% neutral buffered formalin for 48 h, embedded in paraffin, and subjected to hematoxylin–eosin (HE) staining and Masson's trichrome stain, and histopathological changes were observed via a light microscope (Olympus, Japan) to evaluate the pathological damage to the kidneys.

Immunohistochemical and immunofluorescent staining

Paraffin-embedded kidney tissue sections, with a thickness of 4 μm, were prepared for IHC and IF staining. After dewaxing, perform heat-induced epitope retrieval on renal sections, and then were blocked with endogenous peroxidase blocking solution. Subsequently, primary antibodies of α-SMA (Abcam, Cat No.ab5694) and BAX (Proteintech, Cat No.60267-1-Ig) were applied and left to incubate overnight at 4 °C. After three washes with PBS, sections were treated with super horseradish peroxidase (HRP) Mouse/Rabbit IHC Kit (Boster, Beijing,

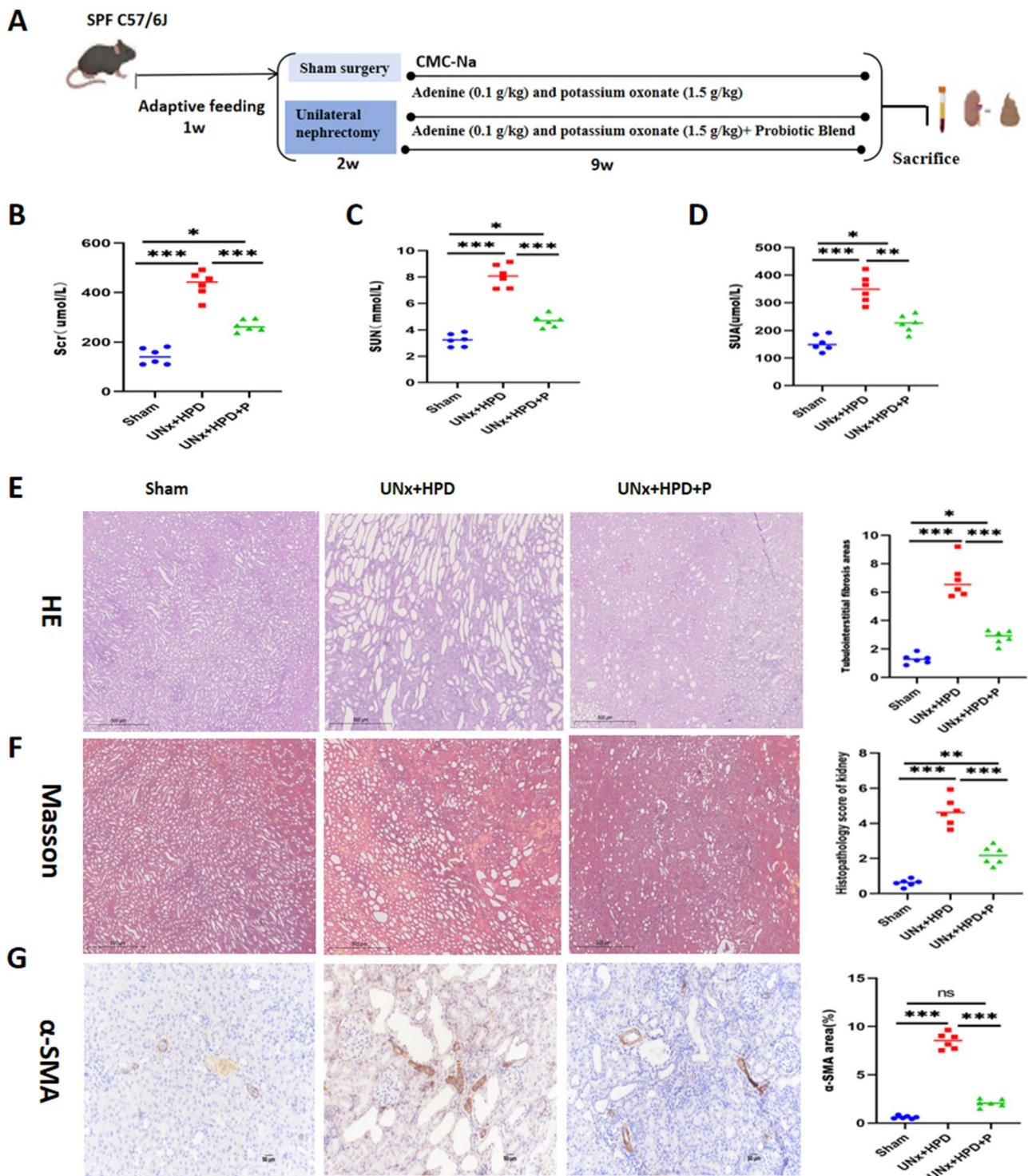


Fig. 1 Effects of mixed probiotics on kidney damage caused by a high-purine diet. **(A)** Schematic experimental design for mixed probiotics intervention. **(B-D)** Alteration of serum creatinine, urea, and uric acid in three groups of mice ($n=6$). The data are expressed as mean \pm SEM ($n=6$); **(E)** Representative kidney tissue sections of three groups. Hematoxylin-eosin (HE) staining; **(F)** Representative kidney tissue sections of three groups Masson's trichrome staining; **(G)** Immunohistochemical staining of SMA in kidney tissues of three groups. * $P < 0.05$, ** $P < 0.01$, *** $P < 0.001$. Analysis was performed by ANOVA followed by Tukey's multiple comparison test

China) according to the manufacturer's instructions. The peroxidase conjugate is visualized using the diaminobenzidine (DAB) kit (Boster, Beijing, China).

Regarding IF, primary antibodies of Beclin-1 (Proteintech, Cat No. 66665-1-Ig), LC3 (Proteintech, Cat No. 14600-1-AP) and Caspase-3 (Proteintech, Cat No. 25128-1-AP), ZO-1 (Proteintech, Cat No. 21773-1-AP) were applied and incubated for 60 min, and then were incubated with FITC-conjugated (green) secondary antibodies (Beyotime, Cat No. A0568) at room temperature for 2 h. Nuclei were stained with DAPI. Photomicrographs were captured using Olympus Provis AX70 microscope (Olympus Corporation, Japan), with analysis conducted using Image J software.

TUNEL fluorescence detection

Dewax and rehydrate the paraffin sections of kidney tissue; treat the tissue with Proteinase K working solution for 15 min at 37 °C; rinse with PBS 3 times; prepare the TUNEL reaction mixture, 50 L of TdT enzyme storage solution, and 450 L of fluorescein-labeled dUTP solution, and mix well; add 50 µL of TUNEL reaction mixture to the specimen, add a coverslip or sealing film, and react in a dark, humid box at room temperature for 30 min. Rinse 3 times with PBS; add 1 drop of anti-fluorescence quenching mounting medium containing DAPI, and count apoptotic cells under a fluorescence microscope.

16 S rRNA sequencing

Fresh feces were collected and transported on dry ice before the mice were sacrificed. The samples were then stored at -80 °C until DNA extraction. The CTAB/SDS method was used to extract DNA from the samples. Check DNA concentration and purity on a 1% agarose gel, then dilute to 1 g/L with sterile water. 338 F (5'-actcctacgggaggcagcag-3') and 806R (5'-ggactachvggggtwtctaat-3') primers amplified 16S rRNA in the V3-V4 region of all samples. PCR products were mixed at equal density and purified using a gel extraction kit. A high-throughput sequencing library was constructed on the Illumina platform and then sequenced using the Illumina NovaSeq platform to generate 250 bp paired-end reads. The FLASH (V1.2.7) platform was used to merge and quality filter raw tags to obtain high-quality sequences on QIIME (V1.9.1). Chimeras were removed using the UCHIME algorithm according to the Silva database. With a limit of 97%, use UPARSE (V7.0.1001) to classify sequences with similarity greater than this limit into the same operational taxonomic units (OTUs). The Silva database was used to annotate taxonomic information of sequences based on the Mothur algorithm. Alpha diversity and beta diversity were calculated using QIIME (V1.7.0). Nonmetric multidimensional scaling (NMDS) analysis was performed on the nonlinear model based on

Bray-Curtis distance using the vegan package in R software (V2.15.3).

Untargeted metabolomics analysis

Fecal samples were subjected to non-targeted metabolomics analysis using liquid chromatography-tandem mass spectrometry (LC-MS/MS). The ultra-high performance liquid chromatography system (Vanquish, Thermo Fisher Scientific) was coupled with a BEH amide column (2.1 mm×100 mm, 1.7 µm) and the Q Exactive HFX mass spectrometer (Orbitrap MS, Thermo) for the separation and extraction of target compounds. Data collected in positive ion mode and negative ion mode were compared with databases (KEGG, HMDB) and analyzed collectively. The extraction of metabolites, LC-MS/MS analysis, data preprocessing, and annotation are detailed in the supplementary materials.

The metabolomics analysis platform (<https://www.metaboanalyst.ca>) was employed for data cleaning, statistical analysis, and pathway enrichment analysis. Peaks were removed, and the peak intensity matrix with zero values in more than 50% of the samples was filtered out. Remaining missing values were replaced with one-fifth of the minimum positive value for each variable. If the relative standard deviation of the deviation value exceeded 25%, those values were filtered out and normalized using the average value. The orthogonal projection to latent structures discriminant analysis (OPLS-DA) algorithm, along with fold change (fc) and t-test, was utilized to identify metabolites with significant differences between groups. Permutation tests (100 permutations) were conducted to validate the OPLS-DA model. Differentially expressed metabolites (DEMs) were identified based on strict criteria: variable importance in projection (VIP) value > 1, $\log_2(\text{fc}) > |2|$, and $p < 0.05$. The Kyoto Encyclopedia of Genes and Genomes (KEGG) pathways of DEMs were enriched using MetaboAnalyst and presented as potential targets with a threshold of $p < 0.05$.

Statistics analysis

All data with normal distributions are presented as mean ± standard deviation (SD). Statistical analyses were performed using GraphPad Prism software (Version 9.5). Continuous data that followed a normal distribution among three groups were analyzed using one-way ANOVA. For continuous data with a non-normal distribution, the Kruskal-Wallis H-test was employed for analysis among the three groups. Unpaired Student's t-tests were utilized to compare two groups, while the Mann-Whitney U-test was applied for nonparametric data. Differential operational taxonomic units (OTUs) were identified using the DESeq2 package, with a threshold of $p < 0.05$ and $\log_2(\text{fold change}) > |1|$. The different bacterial taxa were analyzed by LEfSe. All LEfSe analyses were

performed with false discovery rate (FDR) correction using the Benjamini-Hochberg procedure. Only taxa meeting that met both the LDA score >3 and $q < 0.1$ thresholds were reported as significantly differential. Spearman's correlation analysis was conducted to elucidate potential relationships between key differentially expressed metabolites (DEMs) and parameters associated with chronic kidney disease (CKD). Heatmap and the Sankey bubble plot were visualized by the CNSknowall (<https://cnsknowall.com/>). Statistical notes: ns indicate not significant; * $p < 0.05$; ** $p < 0.01$; *** $p < 0.001$.

Results

Compound probiotic ameliorated a high-purine diet-induced renal injury

The mouse treatment flow chart is presented in Fig. 1A. To evaluate the impact of compound probiotics on kidney damage induced by HUA in the context of CKD, renal function indicators (SUA, Scr and SUN) were measured in mice following a 9-week intervention. The results demonstrated that mice subjected to a high-purine diet exhibited significantly elevated levels of Scr, SUN, and SUA ($p < 0.001$) compared to the control group. After the intervention with compound probiotics, the serum levels of Scr, SUN, and SUA displayed significant reduction ($p < 0.001$) compared with the sham group (Fig. 1B-C). Pathological analysis via HE and Masson staining revealed that renal tissue exhibited tubular vacuolation, atrophy, and interstitial inflammatory infiltration in the UNx+HPD group. However, these renal abnormalities were significantly ameliorated in the probiotic group (Fig. 1D-E). Immunohistochemical staining indicated an increase in the α -smooth muscle actin (α -SMA)-positive area in the UNx+HPD group, while the probiotic group exhibited a markedly reduced SMA-positive area (Fig. 1F). These findings suggest that probiotic intervention can effectively enhance renal function, mitigate tubular damage, and reduce interstitial fibrosis in CKD mice with HUA.

Compound probiotics reduce oxidative stress, mitophagy, and apoptosis induced by a purine-rich diet

Oxidative stress and enhanced mitophagy are recognized as critical mechanisms leading to cell apoptosis in uric acid nephropathy. To assess changes in oxidative stress, the kidney tissue levels of malondialdehyde (MDA) and superoxide dismutase (SOD) were measured by Elisa kit. As shown in Fig. 2A-B, the UNx+HPD group presented an increase in MDA and a decrease in SOD. Notably, after probiotic intervention, there was a significant reduction in MDA ($p < 0.001$) and an increase in SOD ($p < 0.001$), suggesting a potential improvement in oxidative stress associated with HUA and CKD. IF analysis revealed alterations in the expression of mitochondrial

autophagy-related proteins, specifically LC3I/II and Beclin I. The UNx+HPD group exhibited a significant increase in the expression of LC3I/II and Beclin I compared to the sham group, followed by a notable decrease after probiotic intervention (Fig. 2C-D). Additionally,

IHC and IF staining showed that, compound probiotics intervention reduced the expression of Bax, caspase-3 and TUNEL body in the UNx+HPD group (Fig. 2E-G). These findings suggest that probiotic intervention may mitigate mitophagy and apoptosis in kidney tissue induced by elevated uric acid levels.

Alterations of intestinal barrier and gut microbiota upon compound probiotics treatments in UNx+HPD mice

To evaluate the impact of compound probiotics on the intestinal barrier, we utilized immunofluorescence to detect the tight junction protein ZO-1 in the ileum (Supplementary Fig. 1A-B). The level of LPS, an endotoxin from gram-negative bacteria, was highest in the serum of UNx+HPD mice. Compound probiotics significantly reduced plasma LPS levels (Supplementary Fig. 1C).

Next, we explored the structure and differences in the gut microbiota of mice. The α -diversity of the microbiome was estimated, namely, the Chao1 index and OTU reflected the community richness and the Shannon and Simpson index reflected the community diversity. Figure 3A showed that both the OTU ($P = 0.015$) and Chao1 ($P = 0.022$) index displayed a reduction in the UNx+HPD group compared to the sham group, supplementation with compound probiotics increased the alpha diversity indices observed OTU and Chao 1; Nonmetric multidimensional scaling (NMDS) and principal coordinate analysis (PCoA) revealed differences in microbiota structure among the three groups (Figs. 3B-C). Column-stacked plots depict varying levels of taxa at both the phylum and genus levels (Figs. 3D-E). Additionally, Fig. 3F presents a bubble chart that highlights the top 30 differences in phylum and genus levels among the three groups. The five most prevalent phyla identified were *Firmicutes*, *Bacteroidota*, *Patescibacteria*, *Verrucomicrobiota*, and *Proteobacteria*, while the top five genera included *Muribaculaceae_unclassified*, *Candidatus_Saccharimonas*, *Romboutsia*, *Clostridia_UCG-014_unclassified*, and *Streptococcus*.

The histogram of LDA scores (LDA score threshold >3.0) and the cladogram respectively illustrate the classified microbiota of UNx+HPD group and UNx+HPD+P group (Fig. 3G-H). Specifically, *f_Prevotellaceae*, *s_Prevotella_9_unclassified*, *g_Prevotella_9_o_Bacteroidota_unclassified*, *s_Bacteroidota_unclassified*, *g_Bacteroidota_unclassified*, *c_Bacteroidota_unclassified*, *g_Dorea*, *s_Candidatus_Dorea_massiliensis*, *f_Erysipelatoclostridiaceae*, and *f_Anaerofustaceae*, along with *g_Anaerofustis* and *s_Anaerofustis_unclassified*, were

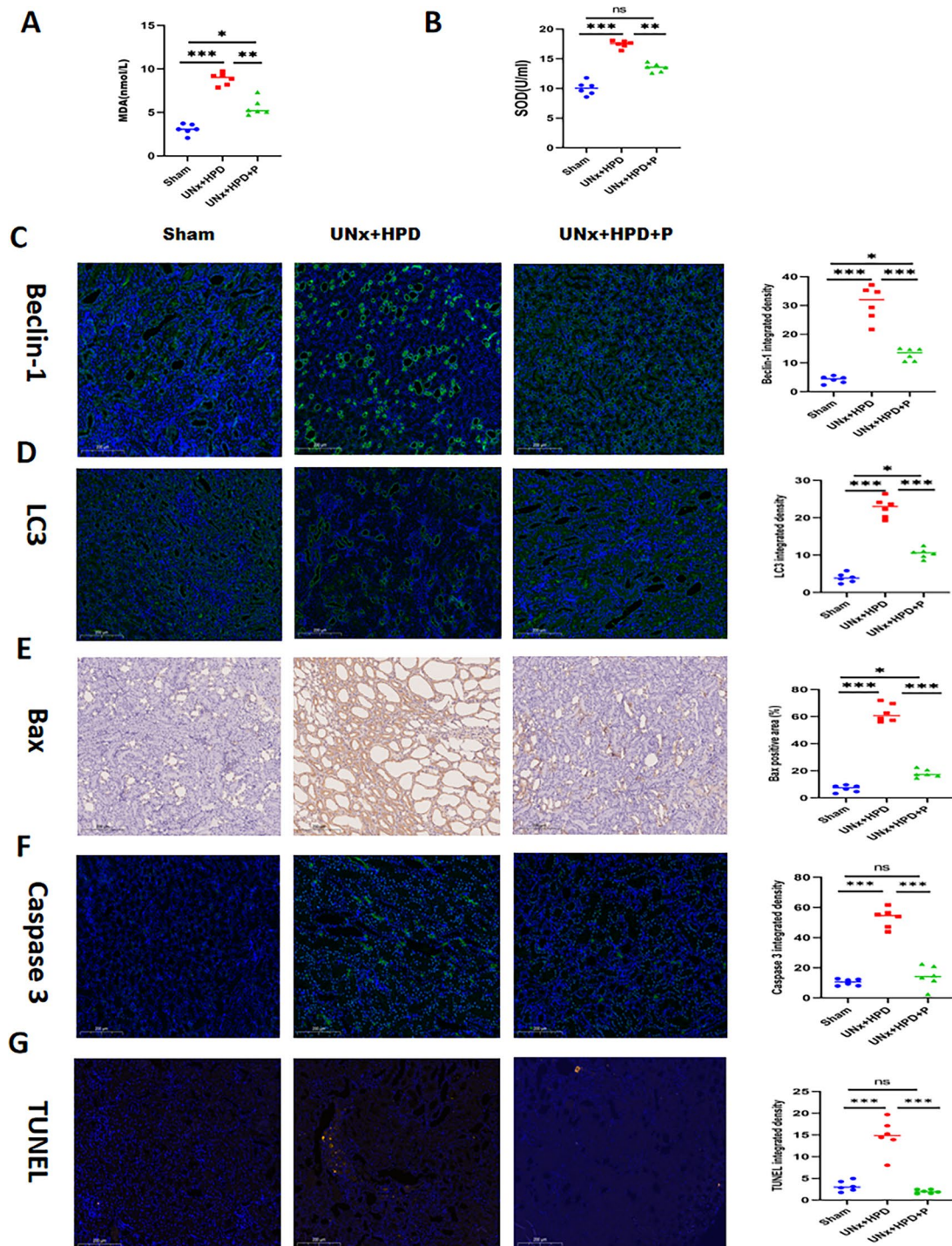


Fig. 2 Effects of mixed probiotics on cell apoptosis, oxidative stress, and mitophagy in renal tissue caused by a high-purine diet. **(A-B)** Concentrations of MDA and SOD in kidney tissue of mice in three groups ($n=6$); **(C)** Immunofluorescence shows the expression of Beclin-1 among the three groups. **(D)** Immunofluorescence shows the expression of LC3 among the three groups. **(E)** Immunohistochemical staining showed mixed probiotics alleviated the upregulation of BAX expression caused by hyperuricemia. **(F)** Immunofluorescence display of mixed probiotics alleviated the upregulation of caspase-3 expression caused by hyperuricemia. **(G)** Immunofluorescence shows the expression of TUNEL among the three groups. * $P < 0.05$, ** $P < 0.01$, *** $P < 0.001$. Analysis was performed by ANOVA followed by Tukey's multiple comparison test. MDA: malondialdehyde, SOD: superoxide dismutase

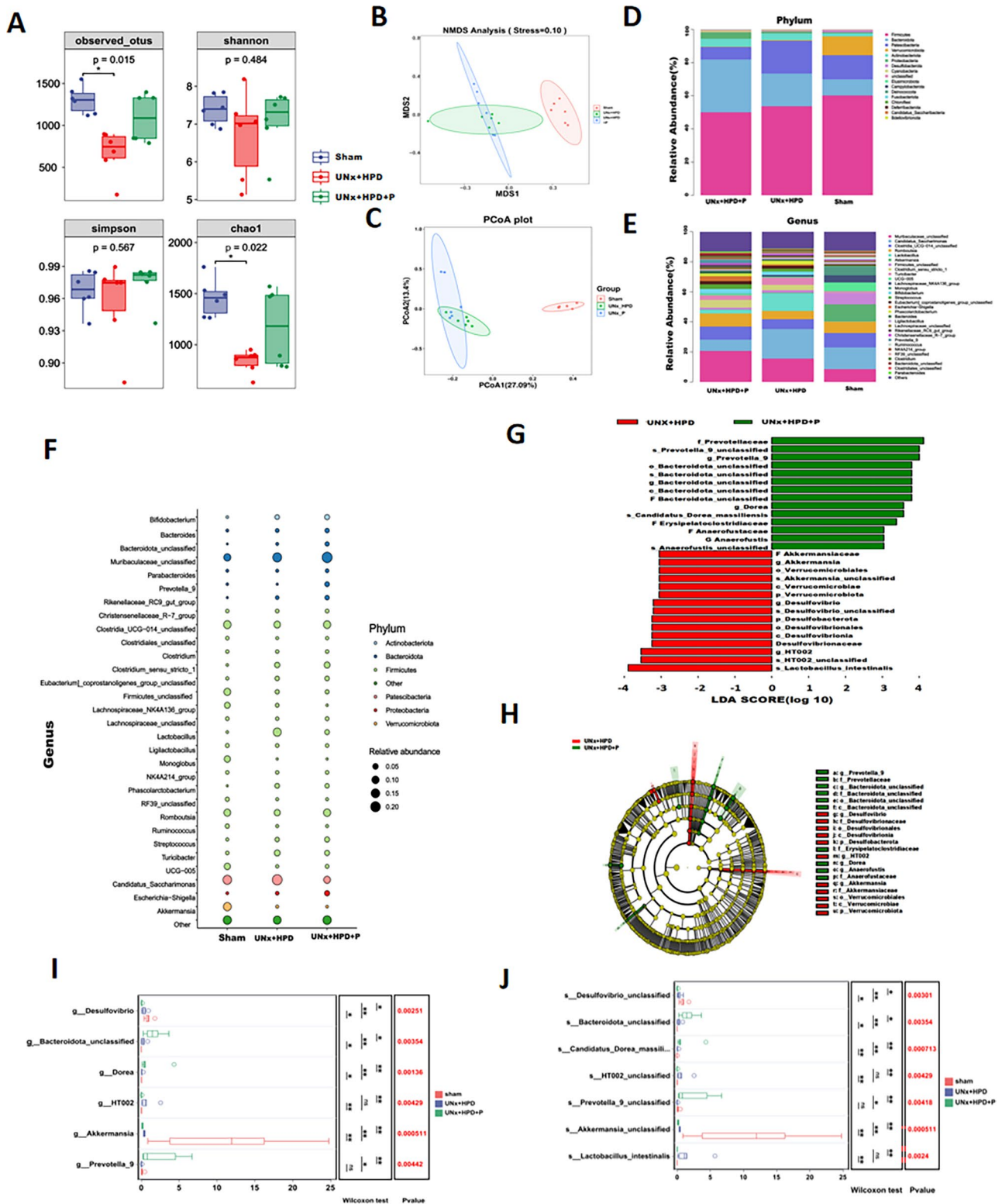


Fig. 3 Altered fecal microbiota after mixed probiotic treatment. **(A)** Alpha diversity boxplot (observed OTUs, Shannon index, Simpson index, Chao1 index). **(B, C)** Principal coordinates analysis (PCoA) and NMDS based on Bray-Curtis distance of **beta diversity**. **(D)** Stacked bar graph showing relative abundance of gut bacteria at phylum level. **(E)** Stacked bar graph showing relative abundance of gut bacteria at genus level. **(F)** The bubble chart shows the differences in the top 30 genus levels of intestinal flora among the three groups. **(G)** LefSe analysis of gut microbiota between UNx+HPD group and UNx+HPD+P group. **(H)** Cladogram of LefSe analysis between UNx+HPD group and UNx+HPD+P group. **(I)** Differences in the genus level among the three groups of bacteria in the LefSe analysis. **(J)** Differences in the specie level among the three groups of bacteria in the LefSe analysis. $P < 0.05$, $**P < 0.01$. Analysis was performed by the Wilcoxon test

more enriched in the UNx+HPD group. In contrast, *f_Akkermansiaceae*, *g_Akkermansia*, *o_Verrucomicrobiales*, *s_Akkermansia_unclassified*, *c_Verrucomicrobiae*, *p_Verrucomicrobiota*, *g_Desulfovibrio*, *s_Desulfovibrio_unclassified*, *p_Desulfobacterota*, *o_Desulfovibrionales*, *c_Desulfovibrionia*, *Desulfovibrionaceae*, *g_HT002*, *s_HT002_unclassified*, and *s_Lactobacillus_intestinalis* were more prevalent in the UNx+HPD+P group than UNx+HPD+group. Subsequently, we conducted an analysis of the bacteria with significant differences among the three groups at both the genus and species levels (Figure I-G). These findings indicate that the diversity of the gut microbiome is lower in the UNx+HPD group, supplementation with compound probiotics can enhance gut microbiota diversity.

Effect of compound probiotics on fecal metabolomics of UNx+HPD mice

To elucidate the mechanisms underlying the renoprotective effects of compound probiotics in UNx+HPD mice, we performed a comprehensive fecal metabolomic analysis by LC-MS/MS. The metabolic profiles were visualized using interactive principal component analysis (PCA), which revealed distinct clustering patterns of fecal metabolites among the three groups. To further display the alterations of the gut microbiome across the experimental groups, DESeq2 was used and visualized in volcano plots with a threshold of $p < 0.05$, $\log_2(\text{fc}) > |1|$ (Figs. 4B–C). Between the sham and UNx+HPD groups, we identified 2,803 differentially expressed metabolites (DEMs), comprising 478 upregulated and 389 downregulated metabolites. These DEMs were predominantly associated with six major metabolic pathways: amino acid metabolism (34.16%), lipid metabolism (12.11%), biosynthesis of amino acids (9.76%), digestive system (9.35%), carbohydrate metabolism (4.88%), and other pathways. Notably, probiotic intervention in the UNx+HPD+P group resulted in 839 DEMs compared to the UNx+HPD group, with 159 metabolites showing increased expression and 436 demonstrating decreased expression. The pathway distribution of these DEMs was characterized by amino acid metabolism (40.64%), lipid metabolism (21.88%), digestive system (9.35%), signaling molecules and interactions (9.38%), and carbohydrate metabolism (6.25%), with additional metabolites distributed across other pathways (Figs. 4D–E).

To explore the functional significance of these DEMs, a metabolic pathway enrichment analysis was conducted using the KEGG database. The metabolic pathways of DEMs between the sham and UNx+HPD groups were identified, including histidine metabolism, ubiquinone and other terpenoid-quinone biosynthesis, tyrosine metabolism, arginine and proline metabolism, and purine metabolism. Furthermore, the metabolic pathways of

DEMs between the UNx+HPD and UNx+HPD+P groups were determined, which included linoleic acid metabolism, vitamin B6 metabolism, arginine and proline metabolism, tyrosine metabolism, glycerolipid metabolism, porphyrin and chlorophyll metabolism, purine metabolism, tryptophan metabolism, and others. The intricate relationships between specific metabolites and their associated pathways were visualized through a Sankey diagram (Figs. 4F–G). Furthermore, hierarchical clustering analysis of pathway-associated metabolites was conducted, with results presented as a heatmap (Fig. 4H, Supplementary Table S1).

Plasma metabolomic alterations induced by compound probiotics in UNx+HPD mice

Global metabolomic analysis was performed on plasma samples using interactive PCA to characterize metabolic profiles across the three experimental groups. Differential metabolites were identified through volcano plot analysis using DESeq2, with significance thresholds set at $p < 0.05$ and $|\log_2(\text{FC})| > 1$ (Fig. 5B–C). Comparative analysis between the sham and UNx+HPD groups revealed 1,381 significantly altered metabolites, comprising 335 upregulated and 205 downregulated metabolites. Pathway enrichment analysis demonstrated that these differential metabolites were primarily associated with six major biological pathways: amino acid metabolism (36.8%), digestive system (22.3%), membrane transport (14.2%), nucleotide metabolism (5.8%), translation (10%), and cancer-related pathways (10.9%). Notably, probiotic intervention in the UNx+HPD+P group resulted in 368 significantly altered metabolites compared to the UNx+HPD group, with 94 upregulated and 95 downregulated metabolites. These metabolites were predominantly enriched in amino acid metabolism (35.6%), cancer pathways (15.6%), lipid metabolism (20%), membrane transport (16.1%), and nervous system-related pathways (13.2%) (Fig. 5D–E).

KEGG pathway enrichment analysis revealed that the pathways exhibiting differential metabolite enrichment between the sham operation group and the UNx+HPD group primarily included aminoacyl-tRNA biosynthesis; glycine, serine, and threonine metabolism; valine, leucine, and isoleucine biosynthesis; acid biosynthesis; biotin metabolism; taurine and hypotaurine metabolism; pyrimidine metabolism; cysteine and methionine metabolism; histidine metabolism; primary bile acid biosynthesis; and glycerophospholipid metabolism. Additionally, significant changes were observed in valine, leucine, and isoleucine degradation; arginine and proline metabolism; and overall amino acid biosynthesis following mixed probiotic treatment (Fig. 5F). As illustrated in Fig. 5G, the Sankey bubble plot concurrently displays the differential metabolites associated with each group of metabolic

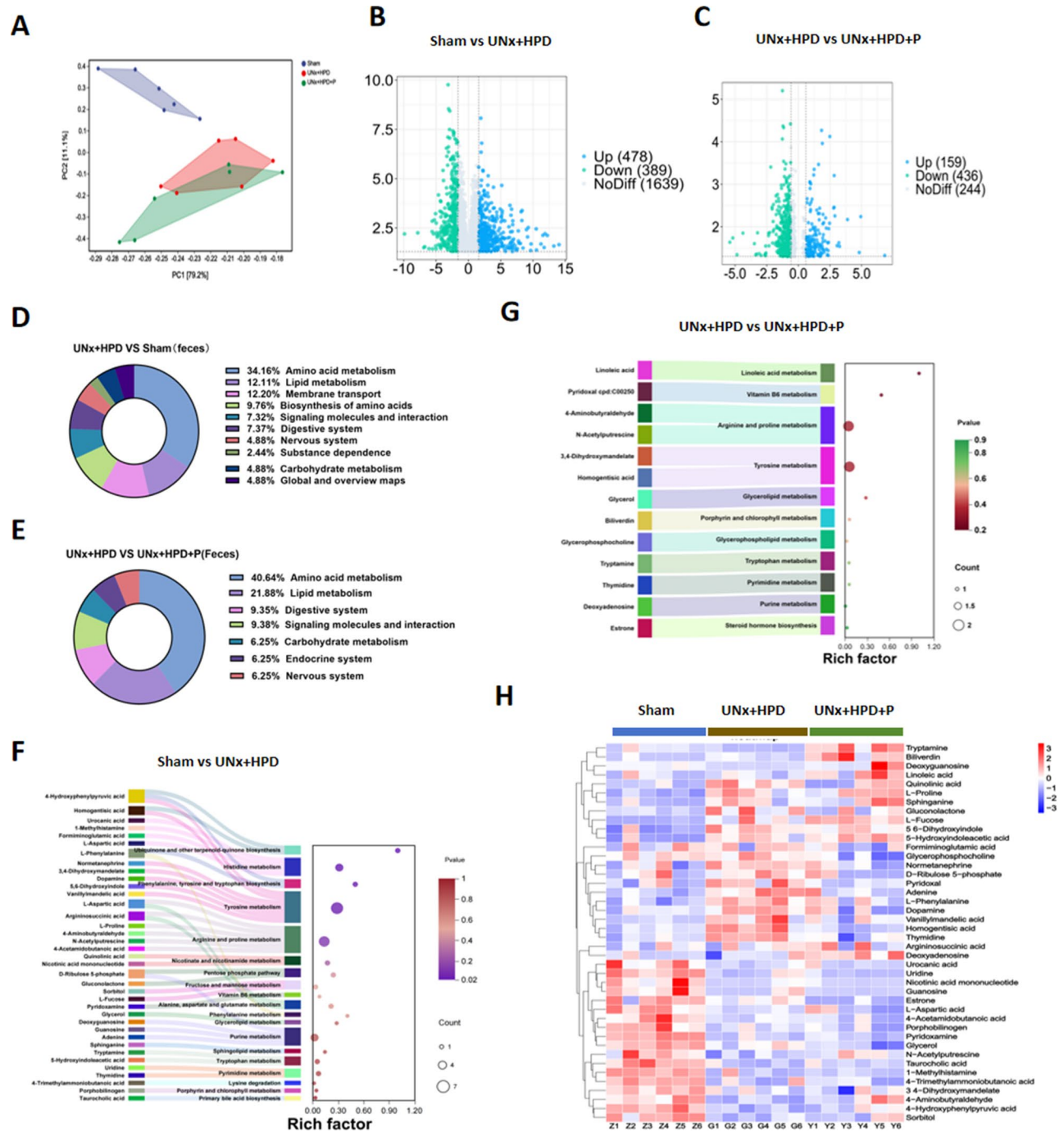


Fig. 4 Altered fecal metabolites after mixed probiotic treatment. **(A)** Interactive principal component analysis of differential metabolites among three groups. **(B)** Volcano diagram showing the DEGs between Sham and UNx+HPD group; **(C)** Volcano diagram showing the DEGs between UNx+HPD and UNx+HPD+P group. **(D)** The pie chart shows the proportion of metabolic categories involved in the KEGG classification of DEGs between Sham and UNx+HPD; **(E)** The pie chart shows the proportion of metabolic categories involved in the KEGG classification of DEGs between UNx+HPD and UNx+HPD+P group; **(F)** The Sankey bubble plot shows the KEGG pathways with differential metabolite enrichment between Sham and UNx+HPD and the DEGs involved in specific pathways. **(G)** The Sankey bubble plot shows the KEGG pathways with differential metabolite enrichment between UNx+HPD and UNx+HPD+P group and the DEGs involved in specific pathways. **(H)** The heatmap presentation of the DEGs among three groups

pathways. Furthermore, hierarchical clustering analysis was conducted to evaluate the expression profiles of pathway-associated metabolites, with results presented as a heatmap (Fig. 5H, Supplementary Table S2).

Integrative metabolomic analysis reveals core metabolites associated with CKD progression

To further investigate the potential mechanistic interactions between compound probiotics and host

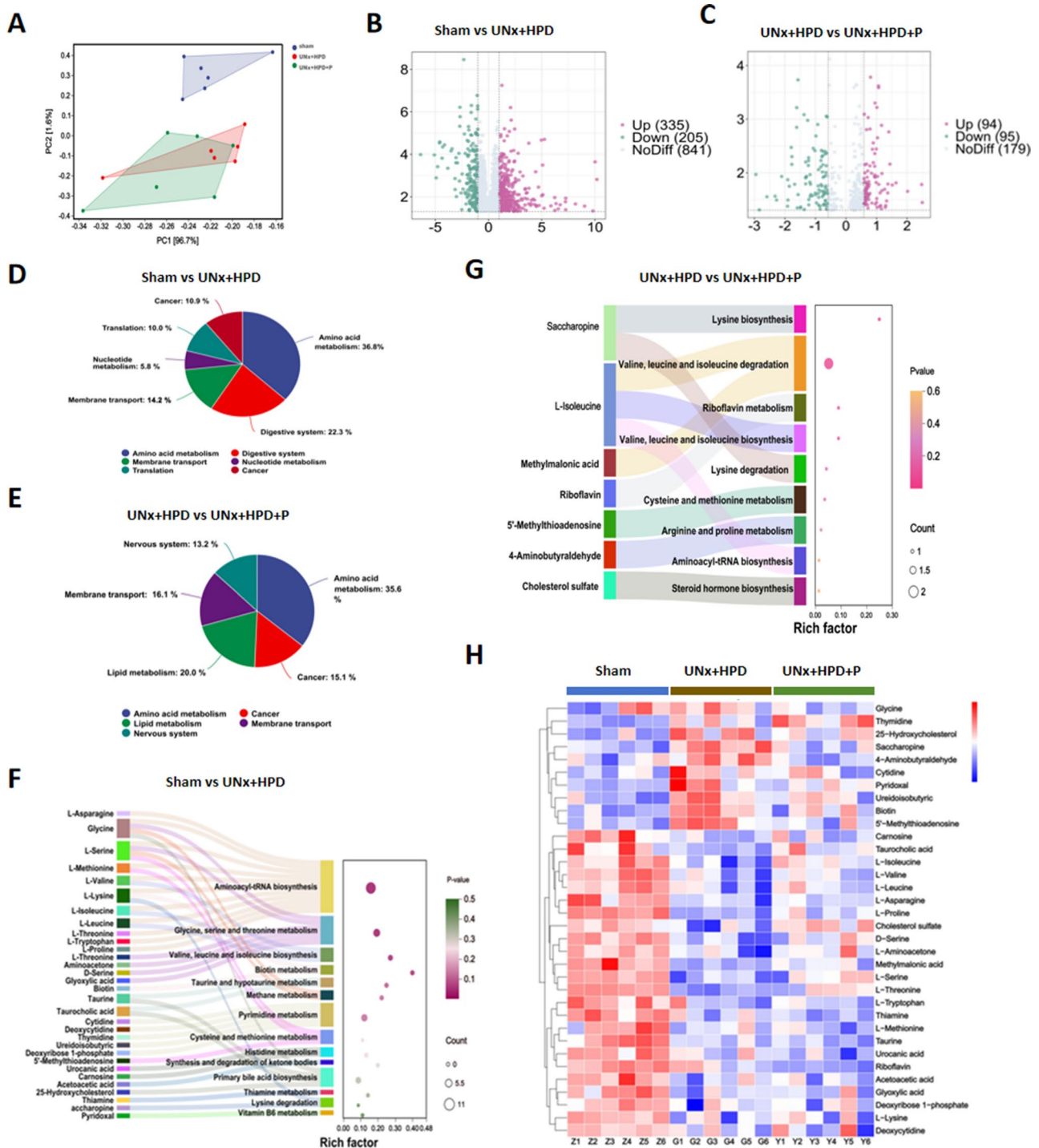


Fig. 5 Altered plasma metabolites after mixed probiotics treatment. **(A)** Interactive principal component analysis of differential metabolites among three groups. **(B)** Volcano diagram showing the DEGs between Sham and UNx+HPD group; **(C)** Volcano diagram showing the DEGs between UNx+HPD and UNx+HPD+P group. **(D)** The pie chart shows the proportion of metabolic categories involved in the KEGG classification of DEGs between Sham and UNx+HPD; **(E)** The pie chart shows the proportion of metabolic categories involved in the KEGG classification of DEGs between UNx+HPD and UNx+HPD+P group; **(F)** The Sankey bubble plot shows the KEGG pathways with differential metabolite enrichment between Sham and UNx+HPD and the DEGs involved in specific pathways. **(G)** The Sankey bubble plot shows the KEGG pathways with differential metabolite enrichment between UNx+HPD and UNx+HPD+P group and the DEGs involved in specific pathways. **(H)** The heatmap presentation of the DEGs among three groups

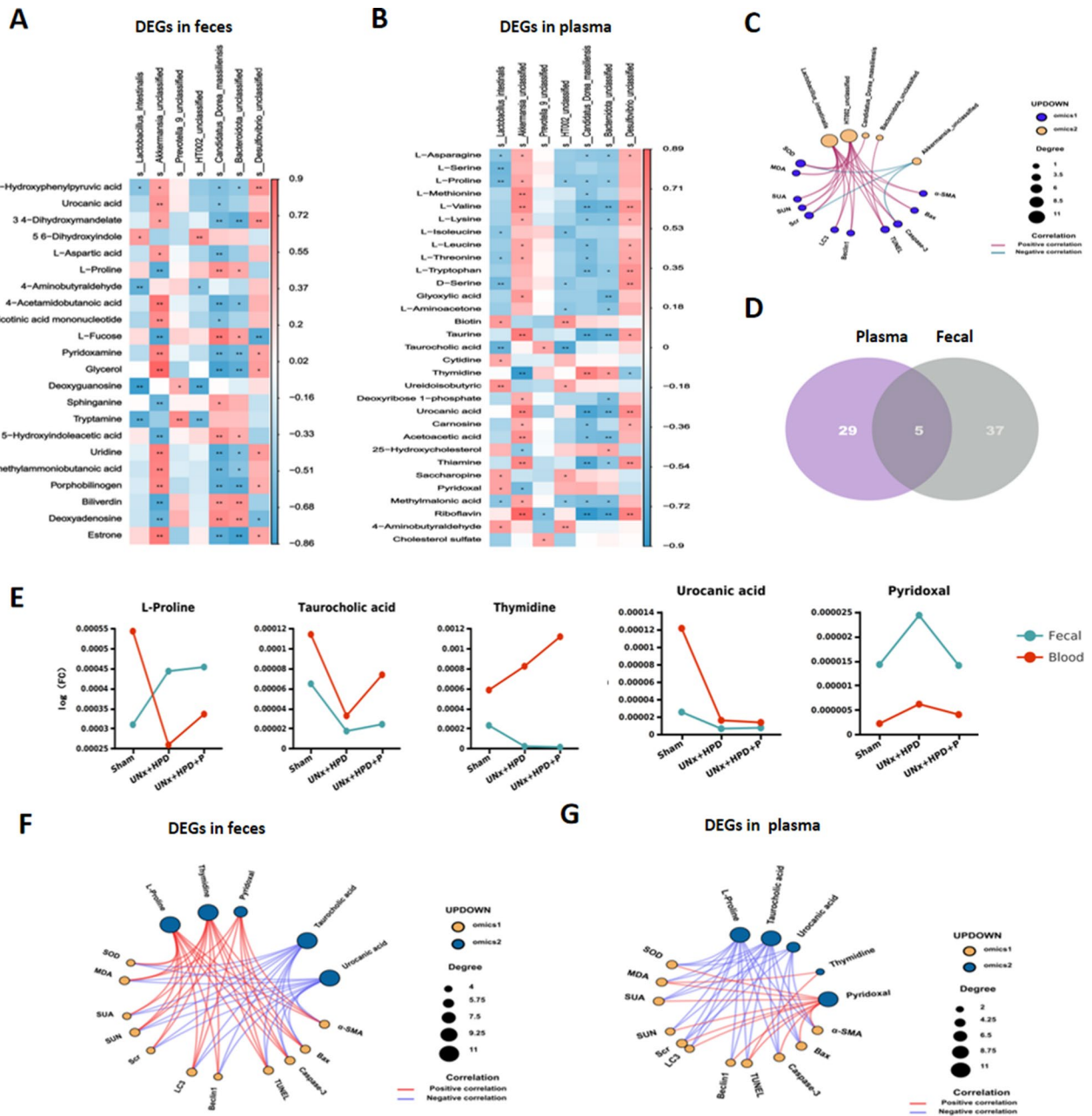


Fig. 6 Correlation between different bacterial species, different metabolites, renal function, oxidative stress, autophagy, and apoptosis indicators. **(A)** Correlation between key differential bacteria and DEGs in feces among three groups. Red indicates a positive correlation. Blue indicates negative correlation. * $P < 0.05$; **(B)** Correlation between key differential bacteria and DEGs in blood among three groups. Red indicates a positive correlation. Blue indicates negative correlation. * $P < 0.05$; **(C)** Correlation network diagram of key differential bacterial groups and related indicators; **(D)** Venn diagram showing the distribution of DEGs in feces and blood involved in KEGG pathways; **(E)** Distribution line chart of differential metabolites shared by feces and blood among the three groups; **(F)** Correlation between five common DEGs in feces and related indicators among the three groups; **(G)** Correlation between five common DEGs in blood and related indicators among the three groups. All network correlations were analyzed using ANOVA, * $P < 0.05$

metabolism, we conducted a Spearman correlation analysis to identify associations between significantly altered metabolites (both fecal and plasma) and key bacterial taxa. As illustrated in Fig. 6A, *Akkermansia unclassified* and *Desulfovibrio unclassified* exhibited positive correlations with various fecal metabolites. For instance, *Akkermansia bacteria* were positively

related to 4-hydroxyphenylpyruvic acid, urocanic acid, 4-aminobutyraldehyde, uridine, thymidine, and pyridoxamine, among others. In contrast, *Lactobacillus intestinalis* showed a negative correlation with 4-aminobutyraldehyde and thymidine. Additionally, *Candidatus_Dorea massiliensis* and *Bacteroidota unclassified* were negatively correlated with pyridoxamine, glycerol,

4-trimethylammoniobutanoic acid, and phosphobilinogen. Regarding plasma metabolites, *Akkermansia_unclassified* and *Desulfovibrio_unclassified* were positively correlated with multiple plasma metabolites, while *Lactobacillus_intestinalis*, *Candidatus_Dorea_massiliensis*, and *Bacteroidota_unclassified* were negatively correlated with several metabolites (Fig. 6B). Furthermore, we aim to explore the associations between key bacterial species and clinically relevant CKD parameters, including renal function markers and inflammatory mediators. Intriguingly, *Akkermansia_unclassified* was found to be negatively correlated with kidney function parameters and inflammatory factors, whereas the remaining four bacterial species exhibited positive correlations with these clinical indicators, as depicted in Fig. 6C.

Venn diagram analysis identified five conserved differential metabolites present in both fecal and plasma samples across all experimental groups: L-proline, taurocholic acid, thymidine, urocanic acid, and pyridoxal (Fig. 6D). These core metabolites may represent critical mediators in the progression of hyperuricemia-induced renal injury. Longitudinal analysis of metabolite profiles demonstrated distinct concentration patterns across biological compartments: taurocholic acid, urocanic acid, and pyridoxal showed consistent directional changes in both fecal and plasma samples, while thymidine exhibited inverse concentration trends between these compartments (Fig. 6E). Network correlation analysis revealed significant associations between these core metabolites and CKD-related parameters. Specifically, thymidine and pyridoxal concentrations in both plasma and feces showed positive correlations with CKD progression markers. Conversely, taurocholic acid and urocanic acid demonstrated negative correlations with these parameters. Interestingly, L-proline displayed compartment-specific associations, showing positive correlations in fecal samples but negative correlations in plasma (Fig. 6F-G).

Discussion

Oxidative stress, mitophagy disorders, and apoptosis resulting from mitochondrial dysfunction are the primary mechanisms underlying renal injury associated with chronic hyperuricemia [23]. Research involving intestinal bacterial transplantation has demonstrated that after renal ischemia/reperfusion (I/R) surgery, mice recolonized with HUA microbiota exhibit severe renal injury and impaired intestinal barrier function [24]. Numerous studies have documented the urate-lowering effects of lactic acid bacteria. Specifically, the oral administration of *Lactobacillus paracasei* has been shown to ameliorate hyperuricemia and the resultant renal damage while concurrently inhibiting the pro-inflammatory cytokine IL-1 in the kidneys [13]. Given that various bacterial species compete for survival within the intestinal environment,

the treatment outcomes with one or more specific strains may vary due to differing survival rates. In this study, a combination of *bifidobacteria*, diverse *lactobacilli*, and prebiotics was employed to intervene in a model of hyperuricemic renal injury. Findings indicate that mixed probiotic treatments can enhance kidney function and mitigate interstitial fibrosis in mice. This conclusion is further corroborated by additional research; for instance, Zhu et al. [25] reported significant reductions in Scr and BUN levels following the oral administration of *Lactobacillus rhamnosus* L34 to 5/6S nephrectomized mice. Guo et al. [26] reported that the intervention with *Lactobacillus reuteri* TSR332 significantly reduced serum uric acid (SUA) levels in hyperuricemic (HUA) rats by approximately 60%, with no notable side effects observed. Additionally, Fernando et al. [27] demonstrated that feeding HUA mice a diet supplemented with probiotics effectively diminished uric acid accumulation. Specifically, *Lactococcus D2022* was found to alleviate HUA and HUA-induced nephropathy by enhancing short-chain fatty acid (SCFA) production in both the intestine and systemic metabolism. Furthermore, probiotics were shown to mitigate symptoms of kidney damage and elevated uric acid levels in mice, indicating their potential to reduce oxidative stress. The antioxidant effects of probiotics were also highlighted in a meta-analysis [28].

As shown previously, multiple studies have indicated that the remodeling of intestinal microbiota could serve as a potential therapeutic approach for managing hyperuricemia and gouty arthritis [29]. In the present study, probiotic intervention led to a significant increase in the abundance of bacterial genera such as *Prevotella_9*, *Dorea*, and *Elusimicrobium* in mice. Conversely, the abundance of genera including *Akkermansia*, *Desulfovibrio*, and *Adlercreutzia* experienced a marked decline. Notably, *Prevotella_9* and *Dorea* are recognized as short-chain fatty acid (SCFA)-producing bacteria [30]. SCFAs are known to inhibit inflammation by reducing the migration and proliferation of immune cells, lowering cytokine levels, and inducing apoptosis [31]. *Akkermansia muciniphila* has demonstrated beneficial effects on various metabolic diseases and has been shown to effectively alleviate hyperuricemia by modulating uric acid metabolism and inflammation [32]. However, it is noteworthy that the abundance of *Akkermansia muciniphila* declined following probiotic intervention. This decrease may be attributed to alterations in the abundance of other bacterial groups, which could create an intestinal environment unfavorable to *Akkermansia muciniphila*'s survival. Our findings revealed a significant reduction in *Desulfovibrio* following a mixed probiotic intervention. *Desulfovibrio*, a thiophagous bacterium, has the potential to promote the synthesis of pro-inflammatory factors ultimately exacerbating the inflammatory response [33].

Indeed, several *Lactobacilli* have been reported to down-regulate *Desulfovibrio*, and the reduction in *Desulfovibrio* in *L. reuteri* DSM 17,938-treated mice was linked to improvements in hepatic steatosis and fibrosis. Furthermore, the longevity effects of *Lactobacillus plantarum* FLPL05 in mice are associated with an increased ratio of *Lactobacilli* to *Desulfovibrio* [34].

Bifidobacteria (e.g., *B. infantis*, *B. longum*) play a significant role in the degradation of purines. Certain bifidobacteria express purine nucleoside phosphorylase, which promotes intestinal purine metabolism and reduces the absorption of uric acid precursors; for instance, *B. adolescentis* has been shown to degrade hypoxanthine in vitro. Additionally, these bacteria exhibit anti-inflammatory effects by secreting short-chain fatty acids (SCFAs), such as butyrate, which inhibit the NLRP3 inflammasome and alleviate renal tubular inflammation [35]. *Lactobacillus casei* contribute to intestinal barrier repair by upregulating tight junction proteins (occludin, ZO-1), thereby reducing the entry of endotoxins (LPS) into the bloodstream and mitigating systemic inflammation [36]. Furthermore, certain strains, such as *L. plantarum*, may modulate intestinal uric acid transporters, promoting fecal uric acid excretion [37]. Metabolic complementarity is observed as *Lactobacillus* ferments dietary fiber to produce lactic acid, which lowers intestinal pH and creates a favorable environment for *Bifidobacterium*. In turn, *Bifidobacterium* converts lactic acid into acetic and propionic acid, synergistically enhancing the anti-inflammatory effects of SCFAs. In terms of immune regulation, *Bifidobacteria* activate regulatory T cells (Treg) through TLR2 signaling, while *lactobacilli rhamnosus* stimulate IL-10 secretion, collectively inhibiting Th17-mediated renal fibrosis [38].

Our previous studies have identified significant differences in fecal metabolism between individuals with chronic kidney disease (CKD) and those with hyperuricemia, particularly in the metabolism of phenylalanine, arginine, proline, purines, and beta-alanine [21]. In alignment with these findings, the present study also investigated non-targeted fecal metabolism in fecal samples. The metabolomic analysis indicated that a greater number of differential metabolites were associated with tyrosine-histidine metabolism, as well as the metabolism of arginine, proline, and purines. These results corroborate the observations of purine metabolism and amino acid biosynthesis in UOX-KO mice. Additionally, alterations in tryptophan metabolism and neuroactive ligand-receptor interactions were partially consistent with previous studies [39]. We observed that mixed probiotic treatment enhanced the metabolism of tyrosine, arginine, and colinine. Tyrosine metabolism is crucial for renal function, as renin produced through this pathway can stimulate the secretion of epinephrine, consequently influencing renal

vasoconstriction and dilation, which affect renal blood flow and filtration rate [40]. The observed lower levels of tyrosine alongside higher levels of its derivatives suggest that mixed probiotic treatment has enhanced the metabolic capacity for tyrosine. Arginine, a semi-essential amino acid, plays a significant role in renal fibrosis. In human proximal tubule cells, spermidine activates nuclear factor erythroid 2-related factor 2 (Nrf2), which inhibits fibrosis and oxidative stress [41]. The biosynthesis of proline occurs in the mitochondria, primarily utilizing glutamic acid derived from glutamine. L-proline has been shown to protect mouse kidneys from aflatoxin-induced oxidative damage and apoptosis [42]. Furthermore, Ac-SDKP treatment has demonstrated potential in improving renal dysfunction and glomerulosclerosis in db/db mice by inhibiting the TGF β /Smad pathway [43].

In the non-targeted metabolomic analysis of serum samples, a greater number of differential metabolites were identified in pathways such as aminoacyl-tRNA biosynthesis, glycine, serine, and threonine metabolism, valine, leucine, and isoleucine biosynthesis, and histidine metabolism, all of which improved following probiotic intervention. Correlation analyses indicated that taurocholic acid and urocanic acid levels in the blood are negatively correlated with renal function parameters, inflammation, oxidative stress, and other related indicators. Probiotics have been shown to increase L-proline levels in the blood, suggesting that L-proline and taurocholic acid may serve as targets for mixed probiotics. According to the literature, the primary physiological role of NADPH in mitochondria is to facilitate the biosynthesis of the non-essential amino acid proline [44]. Additionally, high uric acid levels and mitochondrial dysfunction due to bloodemia may result in decreased proline levels in the bloodstream. Exogenous proline intake has been found to promote cell activation in intestinal lymphoid tissue, thereby playing a crucial role in maintaining intestinal homeostasis and alleviating intestinal inflammation [45]. Taurocholic acid, a product formed from the combination of taurine and cholic acid, has been extensively studied for its mechanism of enhancing antioxidant capacity. Research indicates that taurine supplementation can lead to significant improvements in oxidative stress-related signaling pathways and reduce cell apoptosis, particularly in the context of diabetic kidney injury in rat models [46].

While our findings provide valuable insights, several limitations should be acknowledged. First, the current study primarily establishes correlative relationships rather than causal mechanisms. The precise interactions between specific probiotic strains, their metabolic byproducts, and renal protective effects require further mechanistic investigation through targeted intervention studies. Second, the translational relevance of our

findings from animal models to human patients remains to be established, as interspecies differences in microbial ecology and metabolic responses may influence therapeutic outcomes. Thirdly, the sample size was relatively small, which may limit the generalizability of our findings. This limitation is further compounded by the current paucity of clinical data and well-designed randomized controlled trials.

Conclusions

Compound probiotics supplementation exerts renoprotective effects in hyperuricemia-associated CKD by ameliorating renal function impairment, oxidative stress, mitochondrial dysfunction, and tubular epithelial cell apoptosis. The current metabolomic and microbiome analyses reveal that probiotic intervention effectively restores gut microbial homeostasis and corrects metabolic dysregulation, as demonstrated by significant alterations in both fecal microbiota composition and metabolite profiles. Specifically, we observed substantial perturbations in arginine, proline, and tyrosine metabolism pathways in both fecal and plasma samples from UNx + HPD mice, with probiotic treatment partially normalizing these metabolic alterations, particularly in the plasma compartment. Notably, probiotic intervention significantly up-regulated L-proline levels, and subsequent correlation analysis revealed an inverse relationship between L-proline concentrations and markers of mitochondrial dysfunction and cellular apoptosis. These results suggest that the observed renoprotective effects of probiotics may be mediated, at least in part, through L-proline-mediated attenuation of hyperuricemia-induced oxidative stress and apoptosis pathways.

Supplementary Information

The online version contains supplementary material available at <https://doi.org/10.1186/s12866-025-04012-5>.

Supplementary Material 1

Supplementary Material 2

Supplementary Material 3

Supplementary Material 4

Acknowledgements

We would like to thank Aqu Metabolism Company for its guidance and support in the analysis of intestinal flora and metabolites. Thanks to Zhongke Yikang (Beijing) Biotechnology Co. Ltd. for providing probiotics.

Author contributions

P. Liu and P. Hu. wrote the main manuscript text; MP. Jin, WQ. Sun, J. J. Wu, YY. Tang, DY Shi, T. X.; prepared Figs. 1, 2, 3, 4 and 5 J. Tong, L. Sh. Huang, and D. L. Zhang. were responsible for data analysis., H D He and X D Xu. c completed project design and guidance., H. Zheng, and X D. Xu. provide funding acquisition.

Funding

This work was supported by Shanghai Municipal Science and Technology Commission Project (21dz1200204); Minhang District High-Level Specialty Key Physician Training Program Funding Project (2020MZYS19); Minhang Hospital Affiliated to Fudan University School-level Project Innovation Project (2022MHCX01); Hospital-level discipline-Chronic disease group-Chronic kidney disease project (YJXK-2021-13). Minhang District Central Hospital Top-notch Project (2023MHB04).

Data availability

The 16s rDNA sequencing data can be available in the SRA of NCBI, accession number PRJNA1146380. The metabolomics data can be accessed in OMIX of National Genomics Data Center, under BioProject PRJCA039320.

Declarations

Ethics approval and consent to participate

All animal procedures were approved by the Animal Experimentation Ethics Committee of Fudan University (Approval Number: 2021JS Minhang Hospital-012).

Consent for publication

Not applicable.

Competing interests

The authors declare no competing interests.

Author details

¹Division of Nephrology, Minhang Hospital, Fudan University, No. 170 Xinsong Road, Shanghai 201199, China

²Division of Endocrinology, Minhang Hospital, Fudan University, No. 170 Xinsong Road, Shanghai 201199, China

Received: 1 February 2025 / Accepted: 29 April 2025

Published online: 08 May 2025

References

- Chen-Xu M, Yokose C, Rai SK, Pillinger MH, Choi HK. Contemporary prevalence of gout and hyperuricemia in the united States and decadal trends: the National health and nutrition examination survey, 2007–2016. *Arthritis Rheumatol.* 2019;71(6):991–9. <https://doi.org/10.1002/art.40807>.
- Piao W, Zhao L, Yang Y, et al. The prevalence of hyperuricemia and its correlates among adults in China: results from CNHS 2015–2017. *Nutrients.* 2022;14(19):4095. <https://doi.org/10.3390/nu14194095>.
- Yanai H, Adachi H, Hakoshima M, Katsuyama H. Molecular biological and clinical Understanding of the pathophysiology and treatments of hyperuricemia and its association with metabolic syndrome, cardiovascular diseases and chronic kidney disease. *Int J Mol Sci.* 2021;22(17):9221. <https://doi.org/10.3390/ijms22179221>.
- Madero M, Sarnak MJ, Wang X, et al. Uric acid and long-term outcomes in CKD. *Am J Kidney Dis.* 2009;53(5):796–803. <https://doi.org/10.1053/j.ajkd.2008.12.021>.
- Isaka Y, Takabatake Y, Takahashi A, Saitoh T, Yoshimori T. Hyperuricemia-induced inflammasome and kidney diseases. *Nephrology, Dialysis, Transplantation/Nephrology Dialysis Transplantation.* 2015;31(6):890–6. <https://doi.org/10.1093/ndt/gfv024>.
- Liu N, Wang L, Yang T, et al. EGF receptor inhibition alleviates hyperuricemic nephropathy. *J Am Soc Nephrol.* 2015;26(11):2716–29. <https://doi.org/10.1681/asn.2014080793>.
- Huang ML h., Chiang S, Kalinowski DS, Bae DH, Sahni S, Richardson DR. The Role of the Antioxidant Response in Mitochondrial Dysfunction in Degenerative Diseases: Cross-Talk between Antioxidant Defense, Autophagy, and Apoptosis. *Oxidative Medicine and Cellular Longevity.* 2019;2019:1–26. <https://doi.org/10.1155/2019/6392763>
- Choe JY, Park KY, Kim SK. Oxidative stress by monosodium urate crystals promotes renal cell apoptosis through mitochondrial caspase-dependent pathway in human embryonic kidney 293 cells: mechanism for urate-induced nephropathy. *Apoptosis.* 2014;20(1):38–49. <https://doi.org/10.1007/s10495-014-1057->

9. Che R, Yuan Y, Huang S, Zhang A. Mitochondrial dysfunction in the pathophysiology of renal diseases. *Am J Physiol Ren Physiol/American J Physiol Ren Physiol*. 2014;306(4):F367–78. <https://doi.org/10.1152/ajprenal.00571.2013>.
10. Shi Y, Tao M, Ma X, et al. Delayed treatment with an autophagy inhibitor 3-MA alleviates the progression of hyperuricemic nephropathy. *Cell Death Dis*. 2020;11(6). <https://doi.org/10.1038/s41419-020-2673-z>.
11. Kano H, Yamada N, Saito C, Murayama-Chiba Y, Asami Y, Ito H. Lactobacillus gasseri PA-3, but not L. gasseri OLL2996, reduces the absorption of purine nucleosides in rats. *Nucleosides Nucleotides Nucleic Acids*. 2018;37(6):353–60. <https://doi.org/10.1080/15257770.2018.1469760>.
12. Xiang S, Fu J, Ye K, et al. Effect of Lactobacillus gasseri PA3 on gut microbiota in an in vitro colonic simulation. *Food Sci Nutr*. 2019;7(12):3883–91. <https://doi.org/10.1002/fsn3.1236>.
13. Cao J, Liu Q, Hao H, et al. Lactobacillus paracasei X11 ameliorates hyperuricemia and modulates gut microbiota in mice. *Front Immunol*. 2022;13. <https://doi.org/10.3389/fimmu.2022.940228>.
14. Wang H, Mei L, Deng Y, et al. Lactobacillus brevis DM9218 ameliorates fructose-induced hyperuricemia through inosine degradation and manipulation of intestinal dysbiosis. *Nutrition*. 2019;62:63–73. <https://doi.org/10.1016/j.nut.2018.11.018>.
15. Kuo YW, Hsieh SH, Chen JF, et al. Lactobacillus reuteri TSR332 and Lactobacillus fermentum TSF331 stabilize serum uric acid levels and prevent hyperuricemia in rats. *PeerJ*. 2021;9:e11209. <https://doi.org/10.7717/peerj.11209>.
16. Cao J, Wang T, Liu Y, et al. Lactobacillus fermentum F40-4 ameliorates hyperuricemia by modulating the gut microbiota and alleviating inflammation in mice. *Food Funct*. 2023;14(7):3259–68. <https://doi.org/10.1039/d2fo03701>.
17. Wang Z, Huang Y, Yang T et al. Lactococcus cremoris D2022 alleviates hyperuricemia and suppresses renal inflammation via potential gut-kidney axis. *Food & Function*. Published online January 1, 2024. <https://doi.org/10.1039/d4fo00118d>
18. Li HB, Xu ML, Xu XD, et al. Faecalibacterium prausnitzii attenuates CKD via Butyrate-Renal GPR43 Axis. *Circul Res*. 2022;131(9). <https://doi.org/10.1161/circresaha.122.320184>.
19. Russo E, Viazzi F, Pontremoli R, et al. Association of uric acid with kidney function and albuminuria: the uric acid right for heart health (URRAH) project. *JN J Nephrol*. 2021;35(1):211–21. <https://doi.org/10.1007/s40620-021-00985-4>.
20. Sabatino A, Regolisti G, Brusasco I, Cabassi A, Morabito S, Fiaccadori E, Nephrology, Dialysis. Transplantation/Nephrology Dialysis Transplantation. 2014;30(6):924–33. <https://doi.org/10.1093/ndt/gfu287>.
21. Liu P, Yang J, Chen Y, et al. Alterations of gut microbiota and metabolome in early chronic kidney disease patients complicated with hyperuricemia. *Heliyon*. 2023;9(9):e20328. <https://doi.org/10.1016/j.heliyon.2023.e20328>.
22. Li H, Zhang H, Yan F, et al. Kidney and plasma metabolomics provide insights into the molecular mechanisms of urate nephropathy in a mouse model of hyperuricemia. *Biochim Et Biophys Acta Mol Basis Disease*. 2022;1868(6):166374. <https://doi.org/10.1016/j.bbdis.2022.166374>.
23. Sud M, Tangri N, Levin A, et al. CKD stage at nephrology referral and factors influencing the risks of ESRD and death [J]. *Am J Kidney Dis*. 2014;63(6):928–36.
24. Zhou X, Ji S, Chen L, et al. Gut microbiota dysbiosis in hyperuricaemia promotes renal injury through the activation of NLRP3 inflammasome. *Microbiome*. 2024;12(1). <https://doi.org/10.1186/s40168-024-01826->
25. Tungsanga S, Katavetin P, Panpetch W, et al. Lactobacillus rhamnosus L34 attenuates chronic kidney disease progression in a 5/6 nephrectomy mouse model through the excretion of anti-inflammatory molecules. *Nephrol Dialysis Transplantation*. 2022;37(8):1429–42. <https://doi.org/10.1093/ndt/gfac032>.
26. Xu Y, Cao X, Zhao H et al. Impact of camellia japonica bee pollen polyphenols on hyperuricemia and gut microbiota in potassium oxonate-induced mice [J]. *Nutrients*, 2021, 13(8).
27. Srivastava A, Kaze AD, McMullan CJ, et al. Uric acid and the risks of kidney failure and death in individuals with CKD [J]. *Am J Kidney Dis*. 2018;71(3):362–70.
28. Wang Z, Huang Y, Yang T, et al. Lactococcus cremoris D2022 alleviates hyperuricemia and suppresses renal inflammation via potential gut-kidney axis. *Food Funct*. 2024;15(11):6015–27. <https://doi.org/10.1039/d4fo00118d>.
29. Wang Y, Cai J, Tang C, Dong Z. Mitophagy in acute kidney injury and kidney repair. *Cells*. 2020;9(2):338. <https://doi.org/10.3390/cells9020338>.
30. Wang Z, Li Y, Liao W, et al. Gut microbiota remodeling: A promising therapeutic strategy to confront hyperuricemia and gout. *Front Cell Infect Microbiol*. 2022;12. <https://doi.org/10.3389/fcimb.2022.935723>.
31. Yuan X, Wang L, Bhat OM, Lohner H, Li PL. Differential effects of short chain fatty acids on endothelial Nlrp3 inflammasome activation and Neointima formation: antioxidant action of butyrate. *Redox Biol*. 2018;16:21–31. <https://doi.org/10.1016/j.redox.2018.02.007>.
32. Zhang L, Liu J, Jin T, Qin N, Ren X, Xia X. Live and pasteurized Akkermansia muciniphila attenuate hyperuricemia in mice through modulating uric acid metabolism, inflammation, and gut microbiota. *Food Funct*. 2022;13(23):12412–25. <https://doi.org/10.1039/d2fo0270>.
33. Zhi L, Ang AD, Zhang H, Moore PK, Bhatia M. Hydrogen sulfide induces the synthesis of Proinflammatory cytokines in human monocyte cell line U937 via the ERK-NF- κ B pathway. *J Leukoc Biol*. 2007;81(5):1322–32. <https://doi.org/10.1189/jlb.1006599>.
34. Yu X, Wei M, Yang D, Wu X, Wei H, Xu F. Lactiplantibacillus plantarum strain FLPL05 promotes longevity in mice by improving intestinal barrier. *Probiotics Antimicrob Proteins*. 2022;15(5):1193–205. <https://doi.org/10.1007/s12602-022-09933-5>.
35. Mao H, Fan Y, Tan F, Long X. The effects of Bifidobacterium animalis QC08 on reducing uric acid level and providing renal protection in mice with hyperuricemia. *Front Microbiol*. 2025;16. <https://doi.org/10.3389/fmicb.2025.1529626>.
36. Zhao H, Chen X, Zhang L, et al. Lactocaseibacillus rhamnosus Fmb14 prevents purine induced hyperuricemia and alleviate renal fibrosis through gut-kidney axis. *Pharmacol Res*. 2022;182:106350. <https://doi.org/10.1016/j.phrs.2022.106350>.
37. Shi R, Ye J, Fan H, et al. Lactobacillus plantarum LLY-606 supplementation ameliorates hyperuricemia via modulating intestinal homeostasis and relieving inflammation. *Food Funct*. 2023;14(12):5663–77. <https://doi.org/10.1039/d2fo03411e>.
38. Wang X, Yang S, Li S, et al. Aberrant gut microbiota alters host metabolome and impacts renal failure in humans and rodents. *Gut*. 2020;69(12):2131–42. <https://doi.org/10.1136/gutjnl-2019-319766>.
39. Li H, Zhang H, Yan F et al. Kidney and plasma metabolomics provide insights into the molecular mechanisms of urate nephropathy in a mouse model of hyperuricemia. *Biochimica et Biophysica Acta (BBA) - Molecular basis of disease*. 2022;1868(6):166374. <https://doi.org/10.1016/j.bbdis.2022.166374>.
40. Ragab G, Elshahaly M, Bardin T, Gout. An old disease in new perspective – A review. *J Adv Res*. 2017;8(5):495–doi511. <https://doi.org/10.1016/j.jare.2017.04.00>.
41. Aihara S, Torisu K, Uchida Y, Imazu N, Nakano T, Kitazono T. Spermidine from arginine metabolism activates Nrf2 and inhibits kidney fibrosis. *Commun Biol*. 2023;6(1). <https://doi.org/10.1038/s42003-023-05057-w>.
42. Li H, Li S, Yang H, Wang Y, Wang J, Zheng N. L-Proline alleviates kidney injury caused by AFB1 and AFM1 through regulating excessive apoptosis of kidney cells. *Toxins*. 2019;11(4):226. <https://doi.org/10.3390/toxins11040226>.
43. Shibuya K, Kanasaki K, Isono M, et al. N-Acetyl-Seryl-Aspartyl-Lysyl-Proline prevents renal insufficiency and mesangial matrix expansion in diabetic Db/db mice. *Diabetes*. 2005;54(3):838–45. <https://doi.org/10.2337/diabetes.54.3.838>.
44. Zhu J, Schwörer S, Berisa M, et al. Mitochondrial NADP(H) generation is essential for proline biosynthesis. *Science*. 2021;372(6545):968–72. <https://doi.org/10.1126/science.abd5491>.
45. Wu D, Li Z, Zhang Y, et al. Proline uptake promotes activation of lymphoid tissue inducer cells to maintain gut homeostasis. *Nat Metabolism*. 2023;5(11):1953–68. <https://doi.org/10.1038/s42255-023-00908-6>.
46. Das J, Sil PC. Taurine ameliorates alloxan-induced diabetic renal injury, oxidative stress-related signaling pathways and apoptosis in rats. *Amino Acids*. 2012;43(4):1509–23. <https://doi.org/10.1007/s00726-012-1225-y>.

Publisher's note

Springer Nature remains neutral with regard to jurisdictional claims in published maps and institutional affiliations.